Simulation and design of stable channel-guided laser wakefield accelerators

R. F. Hubbard,[1] D. Kaganovich,[2] B. Hafizi,[3] C. I. Moore,[1] P. Sprangle,[1] A. Ting,[1] and A. Zigler[2]
[1]*Beam Physics Branch, Plasma Physics Division, Naval Research Laboratory, Washington, DC 20375-5346*
[2]*Racah Institute of Physics, Hebrew University, Jerusalem 91904, Israel*
[3]*Icarus Research, Inc., P.O. Box 30780, Bethesda, Maryland 20824-0780*

(Received 4 October 1999; revised manuscript received 2 October 2000; published 27 February 2001)

Most laser wakefield accelerator (LWFA) experiments to date have operated in the self-modulated (SM) regime and have been self-guided. A channel-guided LWFA operating in the standard or resonant regime is expected to offer the possibility of high electron energy gain and high accelerating gradients without the instabilities and poor electron beam quality associated with the SM regime. Plasma channels such as those produced by a capillary discharge have demonstrated guiding of intense laser pulses over distances of several centimeters. Optimizing the performance in a resonant LWFA constrains the on-axis plasma density in the channel to a relatively narrow range. A scaling model is presented that quantifies resonant LFWA performance in terms of the maximum accelerating gradient, dephasing length, and dephasing-limited energy gain. These performance quantities are expressed in terms of laser and channel experimental parameters, clearly illustrating some of the tradeoffs in the choice of parameters. The predicted energy gain in this model is generally lower than that indicated by simpler scaling models. Simulations agree well with the scaling model in both low and high plasma density regimes. Simulations of a channel-guided, self-modulated LWFA are also presented. Compared with the resonant LWFA regime, the requirements on laser and channel parameters in the SM regime are easier to achieve, and a channel-guided SM-LWFA is likely to be less unstable than a self-guided SM-LWFA.

DOI: 10.1103/PhysRevE.63.036502 PACS number(s): 41.75.Jv, 52.38.−r, 52.75.Di, 42.25.Bs

I. INTRODUCTION

Plasma-based accelerators such as the laser wakefield accelerator (LWFA) have demonstrated very large accelerating gradients and acceleration of electrons [1–6] to high energies. In the LFWA, the laser produces a large amplitude plasma wave that moves with the laser pulse and traps and accelerates electrons. The wavelength of the plasma wave is near the plasma wavelength $\lambda_p = 2\pi c/\omega_p$, where the plasma frequency $\omega_p = (4\pi n e^2/m)^{1/2}$, n is the plasma density, and e and m are the electron charge and mass. The plasma density may vary both temporally and spatially, so λ_p is usually calculated based on a nominal on-axis density n_0. The original resonant or ''standard'' laser wakefield accelerator concept [7–10] generally requires the pulse length $c\tau_L$ to be shorter than the nominal plasma wavelength. However, most LWFA experiments to date [1–6] have operated in the highly unstable self-modulated regime where $c\tau_L \gg \lambda_p$, and relativistic focusing [10–14] plays an important role.

Unless the laser beam can be optically guided, the beam will expand quickly due to diffraction. The characteristic distance for the beam to expand due to diffraction is the Rayleigh length Z_R, given by

$$Z_R = \pi r_0^2/\lambda, \tag{1}$$

where r_0 is the radius of the laser beam at the focus. For typical LWFA parameters, diffraction results in a short interaction length that severely limits the energy gain. For example, a recent *unguided* resonant LWFA experiment [15] produced an energy gain of 1.6 MeV, which is far below that observed in the self-modulated experiments [1–6].

Preformed plasma channels, such as those produced by an axicon-focused laser [16–22], a capillary discharge [23–30], or an intense self-guided laser pulse [31], have demonstrated refractive guiding of intense laser pulses over distances of several centimeters. In general, refractive guiding of optical pulses can occur when the index of refraction η peaks on axis. The index of refraction may include contributions from a number of sources, including relativistic [10–14] and atomic [32] self-focusing, preexisting plasma [16–30], and laser-produced plasma [25,28,32–35]. A plasma column with a density variation $n(r)$ introduces a refractive index change $\Delta\eta(r) \approx -\omega_p^2(r)/2\omega_0^2$, where the plasma frequency $\omega_p(r) = [4\pi n(r) e^2/m]^{1/2}$, r is the distance from the axis of the plasma column, and $\omega_0 = 2\pi c/\lambda$ is the laser angular frequency. A plasma column or channel with a density minimum on axis has $\partial\eta/\partial r < 0$ and thus produces the desired refractive index profile for guiding.

In the self-modulated laser wakefield accelerator (SM-LWFA) regime, the laser pulse length is much longer than the wavelength of the plasma wave, and the peak laser power P_0 exceeds the critical relativistic focusing power P_r [10–14]. The critical power in terawatts is given by $P_r(\mathrm{TW}) = 0.017(\lambda_p/\lambda)^2$, where λ is the laser wavelength. The laser pulse is highly unstable, with Raman forward scattering and self-modulation leading to a large amplitude plasma wave that can accelerate electrons to high energies [1–6,12,13,36–39]. Relativistic focusing and ponderomotive expulsion of plasma electrons from the axis provide guiding of the pulse over several Rayleigh lengths [12,13,40]. Experiments have also shown that electrons may be trapped and accelerated directly from the laser-produced plasma without external injection [1–6,38,39]. The high plasma density ($n_0 \sim 10^{19}\,\mathrm{cm}^{-3}$) results in very high accelerating gradients

(>10 GV/m) when the pulse is strongly modulated. Although electron energies above 100 MeV have been reported in some SM-LWFA experiments [4,6], this method is highly unstable and generally produces a poor quality beam with a large energy spread, and thus is likely not to be suitable for a practical accelerator.

This paper presents results on intense laser pulse propagation in plasma channels and assesses the implications for future channel-guided laser wakefield accelerator experiments. A channel-guided LWFA operating in the standard or resonant regime is expected to offer the possibility of high electron energy gain and high accelerating gradients without the instabilities and poor beam quality associated with the self-guided, self-modulated regime. A general analytical scaling model is presented that provides a direct prediction of various LWFA performance quantities in terms of experimental parameters for the laser pulse and plasma channel. Simulations using the LEM (laser electromagnetic) code developed by Krall *et al.* [12] and by Sprangle *et al.* [13] are also presented. LEM is a two-dimensional (2D) axisymmetric simulation code that calculates the laser field and plasma response in a frame moving with the pulse. The code uses the quasistatic approximation and is similar to the WAKE code developed by Antonsen and Mora [41,42].

Section II discusses the basic issues for laser propagation in a preformed density channel. This section includes a review of the standard envelope equation theory, recent experimental results, and simulation. A density channel produced by a capillary discharge provides the guiding in the experiments. This technique was pioneered by Zigler and coworkers [23–28]. The experimental results presented here employed a glass laser with $\tau_L = 400$ fs, $\lambda = 1.06\,\mu$m, and P_0 up to 2.5 TW.

Section III presents an analytical scaling model that can be used to predict the performance of a channel-guided laser wakefield accelerator. The model characterizes LWFA performance based on the maximum accelerating gradient E_m, the dephasing length L_d, and the single stage dephasing-limited energy W_d. The model is cast in terms of six primary experimental parameters: (1) the peak laser power P_0, (2) the laser pulse duration τ_L, (3) the laser wavelength λ, (4) the resonance ratio $\alpha_r \equiv c\tau_L/\lambda_p$, (5) the channel radius $r_{\rm ch}$, and (6) the relative channel depth $\Delta n/n_0$. The matched laser spot size r_M, plasma wavelength λ_p, and laser strength parameter a_0 are also expressed in terms of these primary parameters. The model is restricted to the resonant regime where $\alpha_r < 1$, and makes the *ad hoc* assumption that the peak axial field E_m scales as $E_m \sim \alpha_E \sin \pi\alpha_r$, with $\alpha_E \approx 0.8$. This form is suggested by one-dimensional numerical calculations by Sprangle *et al.* [43] and by Esarey *et al.* [44] and by two-dimensional LEM results reported by Hubbard, Sprangle, and Hafizi [45].

Calculations based on this scaling model are also presented in Sec. III. In this analysis, one of the six primary parameters is varied while the others are held fixed. Since α_r should be ~0.5 to maximize the accelerating gradient, the choice of laser pulse length τ_L constrains the on-axis density to a relatively narrow range and thus has a substantial impact on the choice of channel parameters and LWFA performance quantities.

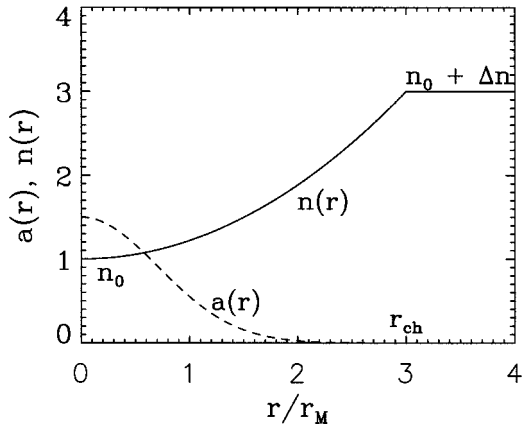

FIG. 1. Idealized radial profiles for the vector potential $a(r)$ and plasma density $n(r)$ for a plasma channel with normalized density $\Delta n/n_0 = 2$ and normalized channel radius $r_{\rm ch}/r_M = 3$.

Section IV presents simulation results for channel-guided laser wakefield accelerators and includes comparisons with the analytical LWFA performance model. Also included are simulations of channel guiding in longer pulse systems ($\alpha_r \gg 1$) that exhibit self-modulation [46]. The channel-guided self-modulated LWFA retains the high accelerating gradients while exhibiting less instability. Results are summarized in Section V.

II. LASER PROPAGATION IN DENSITY CHANNELS

A. Theory of laser spot size evolution in density channels

Laser propagation in a refractive medium can often be described theoretically using an envelope equation formalism [32,47–49] describing the evolution of the spot size r_L. A matched (constant spot size) optical beam can occur if the diffraction term is balanced by the refraction term. In the analysis presented here, the laser pulse is assumed to have a Gaussian radial profile, so that the laser pulse electric field $\mathbf{E}_L$ and vector potential $\mathbf{A}_L$ scale as $\exp(-r^2/r_L^2)$. The laser amplitude is expressed in terms of the normalized vector potential $a = e|\mathbf{A}_L|/mc^2$.

If one includes only the contribution from a parabolic density channel profile $n(r) = n_0 + \Delta n r^2/r_{\rm ch}^2$, where $r_{\rm ch}$ is the channel radius, then the equilibrium or matched beam radius is [10,12]

$$r_M = (r_{\rm ch}^2/\pi r_e \Delta n)^{1/4}, \tag{2}$$

where $r_e = e^2/mc^2$ is the classical electron radius. The radial profiles for the normalized vector potential $a(r)$ and plasma density $n(r)$ are shown in Fig. 1 for an example with $\Delta n/n_0 = 2$ and $r_{\rm ch}/r_M = 3$. The choice of $r_{\rm ch}$ is somewhat arbitrary in practice since the behavior of the laser pulse is insensitive to $n(r)$ for $r \gg r_M$. Figure 1 shows $n(r)$ to be constant for $r > r_{\rm ch}$.

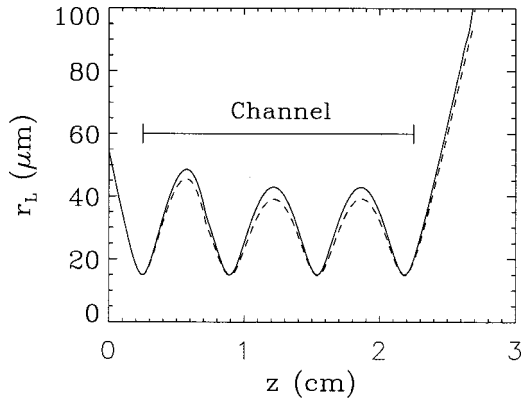

FIG. 2. An example of output from a typical simulation with parameters similar to those in the experiment. The figure plots the laser spot size $r_L(z)$ at the reference point $\zeta^*(z)$ from the simulation. The laser pulse parameters are $\lambda=1.0\,\mu$m, $\tau_L=400$ fs, $r_0=15\,\mu$m, and $P_0=0.035$ TW (solid line) and 0.75 TW (dashed line). The plasma channel is 2 cm long, with channel entrance at $z=0.25$ cm, $r_{\rm ch}=150\,\mu$m, $n_0=5\times10^{18}\,{\rm cm}^{-3}$, and $\Delta n=6\times10^{18}\,{\rm cm}^{-3}$.

If the focused radius r_0 is near the matched beam radius r_M, so that $|r_0-r_M|\ll r_M$, then the spot size $r_L(z)$ undergoes envelope oscillations with a period

$$\lambda_e=\pi Z_M=\pi^2 r_M^2/\lambda. \tag{3}$$

Here $Z_M=\pi r_M^2/\lambda$ is the Rayleigh length associated with the matched beam radius.

B. Simulation of laser guiding in plasma channels

Propagation of laser pulses in plasma channels has been studied with the LEM simulation code. The code was initially developed by Sprangle *et al.* [13] and by Krall *et al.* [12] and is described more fully in the Appendix. LEM is a two-dimensional axisymmetric simulation that calculates laser fields and plasma response in a frame moving with the pulse at the speed of light. The independent variables in the simulation are r, $\zeta=z-ct$, and $\tau=t$, and the code employs the quasistatic approximation and separation of slow and fast time and spatial scales. For convenience, simulation quantities are expressed in terms of z rather than $c\tau$ since the quasistatic approximation is employed, and $z\cong c\tau$ for diagnostics purposes.

Figure 2 shows an example of output from two simulations with parameters similar to those in the experiment described in Sec. II C and illustrates the basic behavior of the laser pulse in the capillary plasma channel. The laser pulse is injected in vacuum at $z=0$ and focused onto the front of the channel. The figure plots the laser spot size $r_L(z)$ at a reference point $\zeta^*(z)$ that moves at the nominal group velocity of the pulse. Both $r_L(z)$ and $\zeta^*(z)$ are more precisely defined in the Appendix. The laser pulse parameters are $\lambda=1\,\mu$m, pulse length $\tau_L=400$ fs, focal spot size $r_0=15\,\mu$m, and peak power $P_0=0.035$ TW (solid line) and 0.75 TW (dashed line). The plasma channel is 2 cm long, with channel entrance at $z=0.25$ cm, channel radius $r_{\rm ch}=150\,\mu$m, peak on-axis density $n_0=5\times10^{18}\,{\rm cm}^{-3}$, and channel depth $\Delta n=6\times10^{18}\,{\rm cm}^{-3}$. The channel density ramps up and down linearly over a distance of 0.1 cm.

As expected, r_L oscillates about an equilibrium value in the channel and expands rapidly once the laser pulse exits the channel. The equilibrium radius r_{Ms} in the low power (0.035 TW) simulation, based on an average of $r_L(z)$ over the three oscillations, is 29.9 μm, while the analytical value for r_M based on Eq. (2) is 25.5 μm. The higher power simulation (dashed line) has a slightly lower value, $r_{Ms}=28.0\,\mu$m. This is probably due to moderate relativistic focusing effects. The oscillation wavelength λ_e based on Eq. (3) is 0.642 cm, while the simulation value $\lambda_{es}=0.646$ cm. A more extensive comparison of simulation and analytical values for r_M and λ_e has been reported previously [28].

The two simulations have substantial differences that are not apparent in Fig. 2. The high power (0.75 TW) simulation exhibits self-modulation within the pulse. For a given value of z, the spot size $r_L(\zeta)$ oscillates in the tail of the pulse, and the amplitude of these oscillations increases with z. The wavelength of oscillations in $r_L(\zeta)$ and other slow time scale quantities such as the axial electric field E_z is close to the plasma wavelength λ_p. Self-modulation in density channels is discussed in more detail in Sec. IV C.

The simulations exhibit a number of phenomena that are not contained in the simple envelope model. For example, the pulse may be distorted due to finite pulse length effects [28,34,50–53], which also cause growth and damping of oscillations in $r_L(z)$ in different potions of the pulse. Pulse distortion and self-steepening due to relativistic modulation effects may also occur [44,54,55]. Further ionization by the intense laser pulse may produce additional plasma near the axis which can interfere with the propagation of the pulse [25,28,35].

C. Experiments on laser guiding in capillary discharge plasma channels

A capillary discharge provides a simple, controllable method for generating a narrow plasma column suitable for laser guiding. In its simplest form, the device consists of a thin cylinder of insulating material such as polyethylene with high voltage electrodes at the ends. The plasma is generated from material ablated from the inner insulating wall of the capillary. The formation of a density minimum on axis has been confirmed experimentally from Stark broadening measurements [25,26]. The radius $r_{\rm ch}$ where the density is at its maximum value is typically 50–70 % of the wall radius r_w.

The laser guiding experiments reported by Zigler *et al.* [23] and by Ehrlich *et al.* [24,25] utilized a linearly polarized Ti: sapphire laser with a 100 fs long pulse at 0.8 μm wavelength and a pulse energy of up to 10 mJ. The pulses were focused onto the entrance of the capillary with a focused spot size of 15 μm. Experiments with 1 cm long cylindrical capillaries [24] demonstrated transport efficiencies of up to 85% in both straight and curved configurations. Laser guiding experiments were also performed in 2, 3, and 6.6 cm long capillaries [25]. Kaganovich *et al.* [26,27] have used a double capillary configuration, which reduces timing jitter

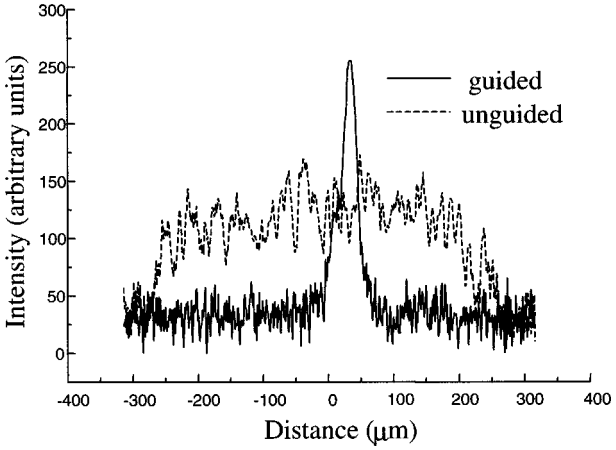

FIG. 3. Plot of the image intensity taken from a lineout of CCD images from a capillary discharge guiding experiment. The guided (discharge-triggered) case has a well-defined narrow peak near the axis, corresponding to a Gaussian spot size $r_L \sim 25\,\mu$m. The unguided (no discharge) case has much lower peak intensity and is relatively uniform.

and allows more control over the plasma density profile

Guiding experiments were also carried out using the NRL T^3 laser. The 1.06 μm wavelength, 400 fs long pulse was focused onto the entrance of the capillary with an initial spot size $r_0 = 15\,\mu$m. The delay time between the initiation of the discharge and the firing of the laser pulse was varied to optimize transport of the pulse. The experimental setup is described in Ref. [27].

Figure 3 shows plots of the image intensity taken from a lineout of charge-coupled device (CCD) images for guided and unguided laser pulses. The laser in this case had 50 mJ of pulse energy and an initial focused intensity of $10^{16}\,\mathrm{W/cm^2}$. In the unguided case, the laser pulse goes through the double capillary, but the discharge is not triggered. The image appears to fill the 250 μm radius capillary. In the guided case, the capillary is triggered to produce the desired plasma channel.

The guided case has a well-defined narrow peak near the axis, corresponding to a Gaussian spot size $r_L \sim 25\,\mu$m. This is based on the spatial width of the pulse at the point where the intensity relative to the baseline drops by e^{-2}. If the channel density peaks at $r_{\mathrm{ch}} = 150\,\mu$m, then a matched radius $r_M = 25\,\mu$m corresponds to a channel depth $\Delta n = 3 \times 10^{18}\,\mathrm{cm^{-3}}$, which is typical of Δn values obtained from Stark broadening. The unguided case exhibits relatively uniform intensity across the capillary.

The energy transfer efficiency for the guided example is 70%, as measured by the laser energy meter. Efficient transfer at higher laser power was also observed and is reported elsewhere [27]. The unguided case showed ~20% transfer efficiency, and may be enhanced by ablation of wall material by the laser itself, forming a reflective layer or shallow plasma channel near the wall that provides a weak guiding effect [27]. Guiding from laser-generated plasma from the walls of a capillary or narrow tube has been observed in a number of experiments, including those of Jackel *et al.* [56] and Korobkin *et al.* [57].

III. ANALYTICAL SCALING OF CHANNEL-GUIDED LWFA PERFORMANCE

A. Model description and assumptions

The channel-guiding experiments and simulations described in the previous section all involved pulse lengths that greatly exceeded the plasma wavelength. If the channel plasma density is reduced, or the pulse length is shortened so that $c\tau_L < \lambda_p$, the requirements for a resonant or ''standard'' laser wakefield accelerator may be satisfied. The intense pulse may produce a large amplitude plasma wake capable of accelerating electrons to high energy in a single stage. This section describes an analytical model that predicts the performance of a channel-guided resonant LWFA in terms of experimental parameters and illustrates some of the tradeoffs in the choice of laser and channel parameters.

1. Choice of primary experimental parameters and performance quantities

The model characterizes the performance of a laser wakefield accelerator by three quantities. The first is the maximum accelerating gradient E_m. High accelerating gradient is clearly desirable for reducing the overall length of the accelerator. A second performance quantity is the dephasing length L_d. This distance determines how long an accelerated electron can remain in phase with the accelerating field without slipping into a decelerating or defocusing part of the wakefield. The quantities E_m and L_d together determine the single stage dephasing-limited energy W_d. Other performance criteria such as particles per beam bunch, beam energy spread, or beam emittance are also important for some applications but are not considered in this analysis.

These three quantities (E_m, L_d, W_d) are usually expressed in analytical models in terms of physical parameters such as the peak laser strength parameter a_0 and the laser and plasma wavelengths λ and λ_p without consideration of the linkage between laser and channel parameters. For example, for a given laser power and plasma channel density, E_m is optimized for a relatively narrow range of laser pulse lengths. In addition, the matched radius r_M is determined entirely by the channel parameters and is generally much larger than the minimum spot size r_0^* to which the laser pulse can be focused.

The model described below casts the three performance parameters (E_m, L_d, W_d) in terms of six primary experimental parameters. These parameters are (1) the peak laser power P_0, (2) the laser pulse duration τ_L, (3) the laser wavelength λ, (4) the resonance ratio $\alpha_r \equiv c\tau_L/\lambda_p$, (5) the channel radius r_{ch}, and (6) the relative channel depth $\Delta n/n_0$. The on-axis density n_0 is thus determined by the pulse length and the resonance ratio. The matched laser spot size r_M, plasma wavelength λ_p, and peak laser strength parameter a_0 may also be expressed in terms of these primary parameters. The model contains an additional free parameter α_E, which scales the peak electric field.

2. LWFA performance model assumptions

The model assumes a linearly polarized laser pulse with a Gaussian radial profile, as described in Sec. II A. The channel has a parabolic density profile given by $n(r)=n_0+\Delta n r^2/r_{\rm ch}^2$. The channel parameters are assumed to be independent of the axial coordinate z, and laser-induced ionization is neglected. The pulse is assumed to propagate at the matched radius r_M given by Eq. (2), which is calculated based on the laser pulse length and channel parameters α_r, $r_{\rm ch}$, and $\Delta n/n_0$. The peak laser strength parameter is then determined by the peak power, laser wavelength, and matched radius. The pulse duration τ_L is based on the full width at half maximum extent of the pulse intensity. With this definition, the maximum accelerating field is obtained when $c\tau_p \approx \lambda_p/2$, or $\alpha_r \approx 0.5$.

Dephasing occurs because an electron moving at axial velocity $v_z \approx c$ will eventually slip out of the accelerating and focusing portion of the wakefield due to the difference between the particle velocity and the wake phase velocity. The phase velocity $\beta_p c$ of the wake is approximately equal to the group velocity $\beta_g c$ of the laser pulse in the plasma channel. If one includes the finite spot size correction to the group and phase velocities [34,45,50–53] and neglects other contributions, then the wake phase velocity is

$$\beta_p = 1-\lambda^2/2\lambda_p^2-\lambda^2/2\pi^2 r_M^2. \tag{4}$$

The normalized slippage rate relative to a particle moving at c is $\Delta\beta_p = 1-\beta_p$, and is appropriate when the relativistic factor γ_e associated with the particle, averaged over the acceleration cycle, is much greater than $\gamma_p=(1-\beta_p^2)^{-1/2}$. Dephasing is assumed to occur when the wake slips by a distance $\lambda_p/4$. The factor of 4 arises because, although one-half of the wake cycle has an accelerating electric field, electrons on the second half of the accelerating cycle experience a defocusing radial electric field that expels them from the channel. The dephasing distance L_d is therefore

$$L_d = \lambda_p/4(1-\beta_p) = \lambda_p/4\Delta\beta_p. \tag{5}$$

If the spot size contribution in Eq. (4) is neglected, one may define the uncorrected laser pulse group velocity (and wake phase velocity) $\beta_{g0}=1-\lambda^2/2\lambda_p^2$. In this case, the uncorrected dephasing length is $L_{d0}=\lambda_p^3/2\lambda^2$, and the phase velocity relativistic factor is $\gamma_p=\lambda_p/\lambda$. However, the spot size correction is frequently important in the regime for LWFAs. The effect is to increase the slippage rate by a factor $(1+\alpha_s)$, where

$$\alpha_s = \lambda_p^2/\pi^2 r_M^2. \tag{6}$$

This effect reduces the dephasing length and the dephasing-limited energy gain. The simple scaling is also modified by a nonlinear correction to the peak electric field that scales as $(1+a_0^2)^{-1/2}$. This correction is retained in the full version of the model discussed below. LEM simulations confirm the importance of retaining both correction terms [45].

B. Derivation of scaling model

1. Derived laser and plasma parameters

The derived laser and plasma parameters include the plasma wavelength λ_p, the corresponding on-axis density n_0, the matched laser spot size r_M, and the laser strength parameter a_0 associated with the peak laser power and matched spot size. In this section, these three parameters are expressed in terms of the primary experimental parameters described above. The parameters are expressed in a form that illustrates the scaling with experimental parameters, and constant coefficients are expressed in cgs units.

Since the resonance ratio α_r characterizing the ratio of the pulse length to the plasma wavelength is $\alpha_r \equiv c\tau_L/\lambda_p$, the plasma wavelength $\lambda_p = c\tau_L/\alpha_r$, and the on-axis density is

$$n_0 = \left(\frac{\pi m}{e^2}\right)\frac{\alpha_r^2}{\tau_L^2} = 1.241\times 10^{-8}\times\frac{\alpha_r^2}{\tau_L^2}. \tag{7}$$

In terms of the primary parameters, the (squared) matched spot size r_M^2 is given by

$$r_M^2 = \left(\frac{c}{\pi}\right)\frac{r_{\rm ch}\tau_L}{\alpha_r(\Delta n/n_0)^{1/2}} = 9.543\times 10^9\frac{r_{\rm ch}\tau_L}{\alpha_r(\Delta n/n_0)^{1/2}}. \tag{8}$$

From this scaling, it is apparent that long pulse length tends to increase the spot size. Although the matched radius given in Eq. (3) is independent of the on-axis density n_0, there are practical limits on how large the normalized channel depth $\Delta n/n_0$ can be. Most current experiments have $\Delta n/n_0 < 1$, but normalized channel depths of 5–10 are likely to be possible in the future. In addition, $r_{\rm ch}$ should be at least a factor of 2 larger than r_M so that the outer edges of the beam do not leak out of the channel.

The squared laser strength parameter a_0^2 is proportional to the peak intensity I_0 and is

$$a_0^2 = \frac{2e^2\lambda^2 I_0}{\pi m^2 c^5} = \frac{4e^2\lambda^2 P_0}{\pi^2 m^2 c^5 r_M^2}, \tag{9}$$

where $I_0 = 2P_0/\pi r_M^2$ for the matched beam radius. In terms of the primary parameters,

$$a_0^2 = \left(\frac{4e^2}{\pi m^2 c^6}\right)\frac{\lambda^2 P_0\alpha_r(\Delta n/n_0)^{1/2}}{r_{\rm ch}\tau_L} = 4.785\times 10^{-28}\frac{\lambda^2 P_0\alpha_r(\Delta n/n_0)^{1/2}}{r_{\rm ch}\tau_L}. \tag{10}$$

The scaling of a_0^2 with $\lambda^2 P_0$ has been noted previously [44]. The remaining scaling with τ_L, α_r, and channel parameters is due to the effect of these parameters on the matched spot size.

2. LWFA performance quantities

The scaling of the derived laser and plasma parameters described above may be incorporated into analytical estimates of the three performance quantities E_m, L_d, and W_d.

In all three cases, the simple scaling assuming $a_0^2 \ll 1$ and $r_M^2 \gg \lambda_p^2/\pi^2$ is presented first, followed by the more general scaling.

The accelerating electric field in a LWFA scales with the characteristic field

$$E_0 = mc\omega_{p0}/e. \tag{11}$$

This quantity is the usual one-dimensional nonrelativistic wave-breaking field. It is often assumed that in the linear regime ($a_0^2 \ll 1$) the peak field for a pulse length near the resonant point ($\alpha_r \approx 0.5$) is given by $E_{m0}^* \approx (a_0^2/2)E_0$. The actual dependence on pulse length is more complicated. Based on numerical solutions to the one-dimensional Poisson equation, Sprangle *et al.* [43] and Esarey *et al.* [44] have shown that the peak field is typically $0.8E_{m0}^*(1+a_0^2/2)^{-1/2}$. For $c\tau_L < \lambda_p$, the variation of E_m with pulse length resembles a sine curve peaked near $c\tau_p = \lambda_p/2$ [43–45]. For this reason, we assume that the uncorrected (small a_0) peak electric field can be approximated by

$$E_{m0} = \alpha_E \sin(\pi\alpha_r) E_{m0}^* = \alpha_E \sin(\pi\alpha_r)(a_0^2/2)E_0, \tag{12}$$

with the scaling factor $\alpha_E \approx 0.8$. The corrected peak field E_m is

$$E_m = \frac{E_{m0}}{(1+a_0^2/2)^{1/2}}. \tag{13}$$

Equation (12) may be rewritten in terms of the primary parameters by noting that $\omega_{p0} = 2\pi\alpha_r/\tau_L$. Equation (12) for the uncorrected peak field becomes

$$E_{m0} = \left(\frac{4e}{mc^5}\right)\frac{\alpha_E \alpha_r^2 \lambda^2 P_0 (\Delta n/n_0)^{1/2} \sin\pi\alpha_r}{r_{\rm ch}\tau_L^2}$$
$$= 8.71\times 10^{-35}\frac{\alpha_E \alpha_r^2 \lambda^2 P_0 (\Delta n/n_0)^{1/2} \sin\pi\alpha_r}{r_{\rm ch}\tau_L^2}. \tag{14}$$

The high intensity correction may be applied using Eq. (13) to obtain E_m.

As noted in Sec. III A 2, the uncorrected (large spot size) dephasing distance is $L_{d0} = \lambda_p^3/2\lambda^2$. In terms of the primary parameters, this distance is

$$L_{d0} = \left(\frac{c^3}{2}\right)\frac{\tau_L^3}{\alpha_r^3\lambda^2} = 1.35\times 10^{-31}\frac{\tau_L^3}{\alpha_r^3\lambda^2}. \tag{15}$$

Applying the spot size correction gives

$$L_d = L_{d0}/(1+\alpha_s). \tag{16}$$

Finally, the dephasing-limited energy W_d is obtained by averaging the electric field over the quarter-cycle dephasing distance. In the linear regime, the wakefield is sinusoidal, so the average accelerating field $\langle E_{z0}\rangle = 2E_{m0}/\pi$. This leads to the usual dephasing limit on energy with relativistic factor γ_{d0} given by

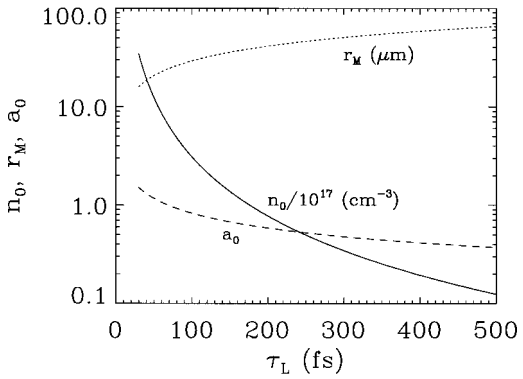

FIG. 4. Derived laser and plasma parameters n_0, r_M, and a_0 versus pulse length τ_L for a typical Ti:sapphire system with $P_0 = 20$ TW, $\lambda = 0.8\ \mu$m, $\alpha_r = 0.5$, $r_{\rm ch} = 100\ \mu$m, and $\Delta n/n_0 = 5$.

$$\gamma_{d0} = 2(E_{m0}/E_0)(\lambda_p^2/\lambda^2). \tag{17}$$

In terms of the primary experimental parameters, the uncorrected energy gain is

$$\gamma_{d0} = \left(\frac{4e^2}{\pi m^2 c^4}\right)\frac{\alpha_E P_0 \tau_L (\Delta n/n_0)^{1/2} \sin\pi\alpha_r}{r_{\rm ch}\alpha_r}$$
$$= 4.38\times 10^{-7}\frac{\alpha_E P_0 \tau_L (\Delta n/n_0)^{1/2} \sin\pi\alpha_r}{r_{\rm ch}\alpha_r}. \tag{18}$$

Applying the finite spot size correction to the dephasing length and the high intensity correction to the electric field, one obtains

$$\gamma_d = \frac{\gamma_{d0}}{(1+\alpha_s)(1+a_0^2/2)^{1/2}}. \tag{19}$$

In the limit $\gamma_d \gg 1$, the dephasing-limited energy is $W_d = mc^2\gamma_d$.

C. LWFA performance model results

The model described in the previous section may be used to predict LWFA performance over a wide range of experimental parameters. To illustrate the scaling, one of the six primary parameters ($P_0, \tau_L, \lambda, \alpha_r, r_{\rm ch}, \Delta n/n_0$) may be varied while the others are held fixed. The derived parameters n_0, r_M, and a_0 are calculated from Eqs. (7), (8), and (10). Equations (13) and (14) determine the peak accelerating field E_m. Equations (15) and (16) give the dephasing length L_d, including the spot size correction, and Eqs. (18) and (19) determine the dephasing-limited energy gain γ_d or W_d. In all of the examples below, the electric field scale parameter $\alpha_E = 0.8$.

1. Scaling with pulse length τ_L

The pulse length τ_L has a substantial impact on the choice of channel parameters, and thus LWFA performance. It is not easy to change this quantity in most laser systems. Figure 4 plots the derived parameters n_0, r_M, and a_0 versus pulse length τ_L for a typical Ti:sapphire system with P_0

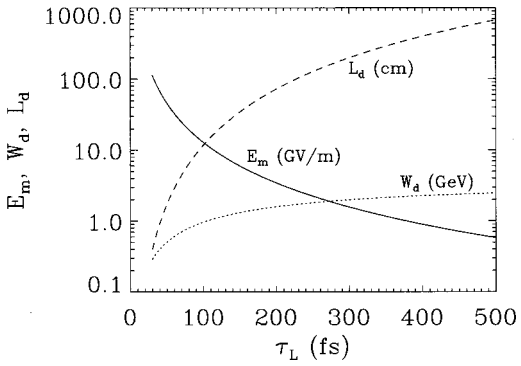

FIG. 5. LWFA performance quantities E_m, L_d, and W_d versus τ_L for the case shown in Fig. 4.

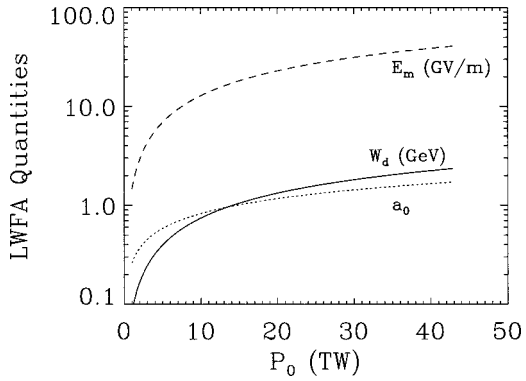

FIG. 6. Peak gradient E_m, dephasing-limited energy gain W_d, and normalized laser potential a_0 versus peak laser power P_0 for a representative short pulse Ti:sapphire LWFA with $\tau_L=100$ fs, $\lambda=0.8\,\mu$m, $\alpha_r=0.5$, $r_{ch}=50\,\mu$m, and $\Delta n/n_0=5$. For these parameters, the on-axis density $n_0=3.10\times10^{17}\,\mathrm{cm}^{-3}$, the matched radius $r_M=20.7\,\mu$m, and the dephasing length $L_d=9.1$ cm.

$=20$ TW, $\lambda=0.8\,\mu$m, $\alpha_r=0.5$, $r_{ch}=100\,\mu$m, and $\Delta n/n_0=5$. The on-axis density n_0 scales as τ_L^{-2} and thus drops dramatically as the pulse length is increased. The on-axis density exceeds $10^{18}\,\mathrm{cm}^{-3}$ for extremely short ($\sim$50 fs) pulses and is two orders of magnitude lower for a 500 fs pulse. Since the normalized channel depth $\Delta n/n_0$ is held constant, the spot size r_M is proportional to $\tau_L^{1/2}$ and thus increases slowly with pulse length. The resulting decrease in intensity is reflected in the $\tau_L^{-1/2}$ scaling of the laser strength parameter a_0.

Figure 5 plots the performance quantities E_m, L_d, and W_d versus τ_L for the case shown in Fig. 4. The primary scaling of the peak accelerating field E_m with pulse length is τ_L^{-2}. Thus, accelerating gradients are much higher with shorter pulse lengths. This scaling is modified slightly by the relativistic $(1+a_0^2/2)^{-1/2}$ correction in Eq. (13). The uncorrected dephasing length L_{d0} scales as τ_L^3 and thus is much larger for long pulse lengths. Since the spot size correction factor α_s increases with τ_L, the scaling of the corrected dephasing length value L_d with τ_L is weakened slightly. The uncorrected dephasing-limited energy gain W_{d0} is proportional to τ_L. The scaling for W_d is modified slightly by the relativistic and finite spot size corrections, which generally cause a somewhat weaker dependence than the simple $W_{d0}\sim\tau_L$ scaling. For long pulses, the dephasing length exceeds 100 cm, so the practical limit on single stage energy is effectively determined by the accelerating gradient.

2. Scaling with laser power P_0

The accelerating electric field E_m and dephasing-limited energy gain W_d are linear in beam power P_0, while $a_0\sim P_0^{1/2}$. The on-axis density, matched spot size, and dephasing length are independent of beam power.

Figure 6 plots E_m, W_d, and a_0 versus P_0 for a representative short-pulse Ti:sapphire LWFA with $\tau_L=100$ fs, $\lambda=0.8\,\mu$m, $\alpha_r=0.5$, $r_{ch}=50\,\mu$m, and $\Delta n/n_0=5$. For these parameters, the on-axis density $n_0=3.10\times10^{17}\,\mathrm{cm}^{-3}$, the matched radius $r_M=20.7\,\mu$m, and the dephasing length $L_d=9.1$ cm. The dephasing-limited energy gain exceeds 1 GeV for $P_0>15$ TW. The accelerating gradient exceeds 10 GV/m in this regime, and $a_0\sim1$. Systems with a few terawatts of laser power are limited to energy gains of a few hundred MeV. The dephasing length is somewhat longer than the 6.6 cm capillary channel length reported by Ehrlich *et al.* [25] but does not appear to be unreasonable. The energy gain in longer channels would presumably be limited by dephasing.

Figure 7 plots the same quantities (E_m, W_d, and a_0) for a longer pulse (400 fs) typical of glass laser chirped pulse amplification (CPA) systems. The experimental parameters are $\lambda=1.0\,\mu$m, $\alpha_r=0.5$, $r_{ch}=100\,\mu$m, and $\Delta n/n_0=5$. This results in on-axis density $n_0=1.94\times10^{16}\,\mathrm{cm}^{-3}$, matched radius $r_M=58.4\,\mu$m, and dephasing length $L_d=255$ cm. The dephasing-limited energy gain is significantly higher than in the previous case, but the long dephasing length is well beyond present channel generation capabilities. The accelerating gradient is ''modest,'' with $E_m=1.35$ GV/m for a 20 TW system. One reason for this is the lower value of the characteristic field E_0. Since $E_0\sim n_0^{1/2}\sim\tau_L^{-1}$, this field is a factor of 4 lower than in the 100 fs case. The accelerating field is further reduced by the larger spot size, which reduces a_0. The spot size effect causes the overall scaling of E_m with pulse length [Eq. (14)] to behave as τ_L^{-2}.

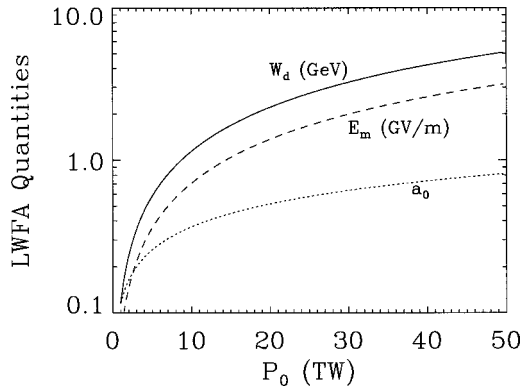

FIG. 7. Plots of E_m, W_d, and a_0 for a longer pulse (400 fs) LWFA. The experimental parameters are $\lambda=1.0\,\mu$m, $\alpha_r=0.5$, $r_{ch}=100\,\mu$m, and $\Delta n/n_0=5$. This results in on-axis density $n_0=1.94\times10^{16}\,\mathrm{cm}^{-3}$, matched radius $r_M=58.4\,\mu$m, and dephasing length $L_d=255$ cm.

3. Scaling with other primary parameters

The relative channel depth $\Delta n/n_0$ and channel radius $r_{\rm ch}$ play a role in determining the matched radius r_M and thus affect a_0, E_m, and W_d. The dependence of r_M and a_0 on the relative channel depth is weak, with $r_M \sim (\Delta n/n_0)^{-1/4}\, r_{\rm ch}^{1/2}$ and $a_0 \sim r_M^{-1}$. The uncorrected electric field E_{m0} and dephasing-limited energy gain W_{d0} both scale as $(\Delta n/n_0)^{1/2}\, r_{\rm ch}^{-1}$. The corrected quantities E_m and W_d vary somewhat more slowly with relative channel depth.

Performance scaling with the resonance ratio α_r comes primarily with its effect on the plasma density, with $n_0 \sim \alpha_r^2$ from Eq. (7). Higher densities lead to smaller spot sizes, with $r_M \sim \alpha_r^{-1/2}$. The scaling of the uncorrected performance quantities is given in Eqs. (14), (15), and (18), with $E_{m0} \sim \alpha_r^2 \sin \pi\alpha_r$, $L_{d0} \sim \alpha_r^{-3}$, and $\gamma_{d0} \sim \alpha_r^{-1} \sin \pi\alpha_r$. The dependence on laser wavelength comes about through the $a_0 \sim \lambda$ scaling in Eq. (9) and the $L_{d0} \sim \lambda^{-2}$ scaling of the dephasing length [Eq. (15)]. This results in an $E_{m0} \sim \lambda^2$ scaling for the uncorrected accelerating gradient, and a dephasing-limited energy gain that is actually independent of laser wavelength. Again, the corrected values are modified by the finite spot size correction to the slippage rate and the large a_0^2 correction to the electric field.

IV. SIMULATION OF CHANNEL-GUIDED LWFA PERFORMANCE

A. Standard LWFA simulation examples

In this section, LEM simulations of channel-guided laser wakefield accelerators are presented. The pulse is injected with initial Gaussian radius $r_0 \approx r_M$ and is allowed to propagate self-consistently in the channel.

The 400 fs scaling example shown in Fig. 7 is typical of present glass laser CPA systems. A LEM simulation was carried out with $P_0 = 19\,\mathrm{TW}$, $n_0 = 1.94 \times 10^{16}\,\mathrm{cm}^{-3}$, $r_{\rm ch} = 140\,\mu\mathrm{m}$, $r_0 = 60\,\mu\mathrm{m}$, $\Delta n/n_0 = 10$, $\tau_L = 400\,\mathrm{fs}$, and $\lambda = 1\,\mu\mathrm{m}$. This choice of parameters corresponds to the nominal optimum resonance ratio ($\alpha_r = 0.5$) for acceleration. Figure 8 shows examples of code results at $z = 10.8\,\mathrm{cm}$. The plot of the instantaneous spot size $r_L(\zeta)$ in Fig. 8(a) shows almost no variation within the pulse, and the spot size is very close to the matched value ($r_M = 58.4\,\mu\mathrm{m}$) given in Eq. (2). There is almost no group velocity slippage of the pulse, which is to be expected since z is much less than $L_d = 255\,\mathrm{cm}$ from Eqs. (15) and (16). The axial electric field $E_z(r,\zeta)$ is shown in the surface plot of Fig. 8(b). Maximum acceleration occurs at $r = 0$ and $\zeta = -230$, where the field amplitude (designated by E_{ms}) is 0.95 GV/m. Acceleration occurs for $E_z(r,\zeta) < 0$. The analytical scaling model predicts a somewhat higher value ($E_m = 1.25\,\mathrm{GV/m}$) for this case. For a fixed laser power and pulse length, the peak field in the simulations is relatively insensitive to modest changes in the on-axis density, provided that Δn (and thus r_M) is held constant.

A modest reduction in the pulse length may lead to substantially higher accelerating gradients. The example below has $\tau_L = 167\,\mathrm{fs}$, $P_0 = 10\,\mathrm{TW}$, $n_0 = 2 \times 10^{17}\,\mathrm{cm}^{-3}$, $\Delta n/n_0 = 5$,

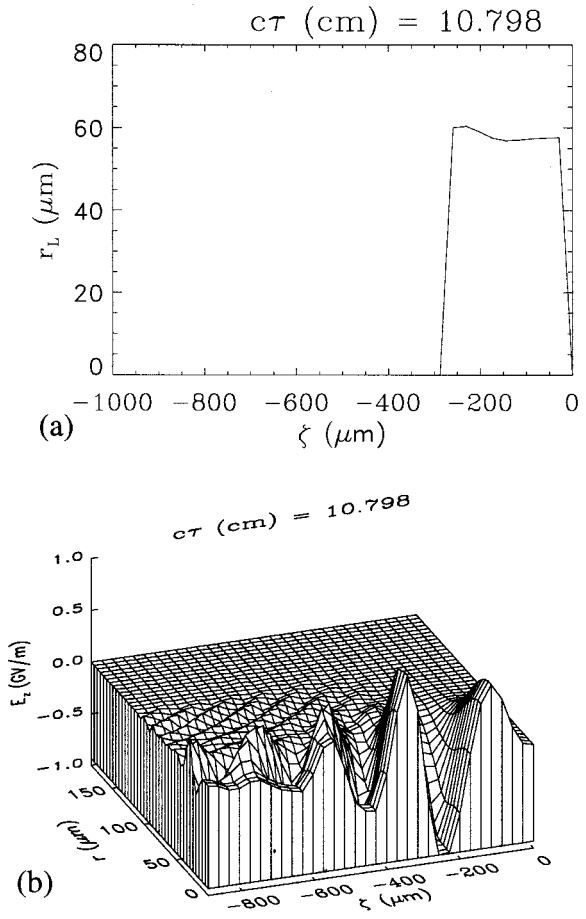

FIG. 8. Simulation results for a long pulse LFWA with $P_0 = 19\,\mathrm{TW}$, $n_0 = 1.94 \times 10^{16}\,\mathrm{cm}^{-3}$, $r_{\rm ch} = 140\,\mu\mathrm{m}$, $r_0 = 60\,\mu\mathrm{m}$, $\Delta n/n_0 = 10$, $\tau_L = 400\,\mathrm{fs}$, and $\lambda = 1\,\mu\mathrm{m}$. The instantaneous spot size $r_L(\zeta)$ at $z = 10.8\,\mathrm{cm}$ shows almost no variation within the pulse, and the spot size is very close to the matched value ($r_M = 58.4\,\mu\mathrm{m}$) given in Eq. (2). The axial electric field $E_z(r,\zeta)$ is shown in the surface plot of (b). Maximum acceleration occurs at $r = 0$ and $\zeta = -230\,\mu\mathrm{m}$, where the field amplitude (designated by E_{ms}) is 0.95 GV/m.

$r_{\rm ch} = 100\,\mu\mathrm{m}$, and $r_0 = 30\,\mu\mathrm{m}$. Figure 9 shows contours of laser intensity $I(r,\zeta)/I_0$ or, equivalently, $a^2(r,\zeta)/a_0^2$ at two different propagation distances. The contour levels are logarithmic between 0.001 and 1. At $z = 1.5\,\mathrm{cm}$ [Fig. 9(a)], the contours show little distortion. However, at $z = 7.5\,\mathrm{cm}$ [Fig. 9(b)], the tail of the pulse ($\zeta \approx -100\,\mu\mathrm{m}$) exhibits significant expansion and distortion, and there is a modest pinching of the pulse at $\zeta = -60\,\mu\mathrm{m}$. The distortion in the tail is due to the finite pulse length effects discussed in Refs. [28], [50–53], while the pinching is due to relativistic focusing. Group velocity slippage of the pulse is also apparent, with the head of the pulse having moved approximately 10 μm in the speed of light coordinate system in propagating 7.5 cm.

Surface plots of the electric field at $z = 1.5$ and 7.5 cm are shown in Fig. 10. The simulation exhibits a well-defined wakefield suitable for acceleration. The peak accelerating gradient $E_{ms} = 5.5\,\mathrm{GV/cm}$ averaged over an envelope oscillation cycle. Based on the slippage rate in the simulation, the quarter-cycle dephasing length $L_{ds} = 13.4\,\mathrm{cm}$. The energy

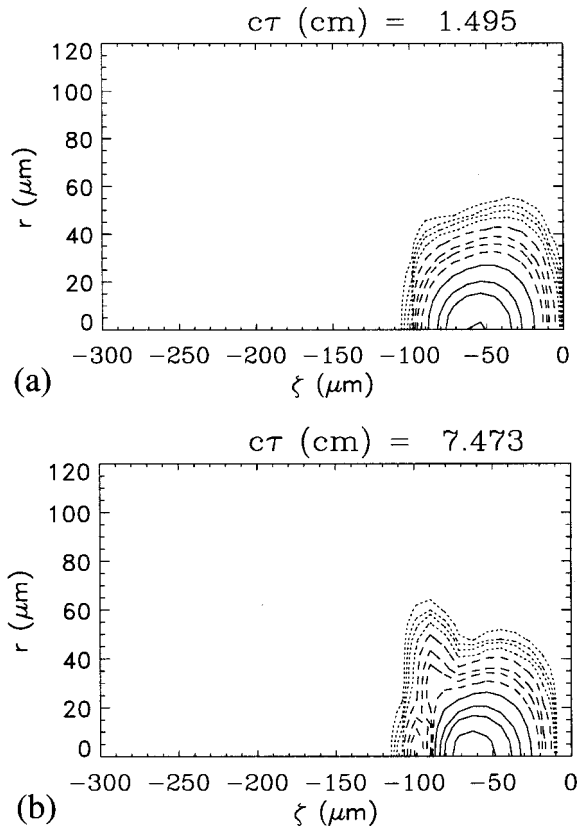

FIG. 9. Contours of laser intensity $I(r,\zeta)/I_0$ or, equivalently, $a^2(r,\zeta)/a_0^2$ at two different propagation distances ($z=1.5$ and 7.5 cm). The LWFA simulation parameters are $\tau_L=167$ fs, $P_0=10$ TW, $n_0=2\times10^{17}\,\mathrm{cm}^{-3}$, $\Delta n/n_0=5$, $r_{\mathrm{ch}}=100\,\mu$m, and $r_0=30\,\mu$m. The contour levels are logarithmic between 0.001 and 1.

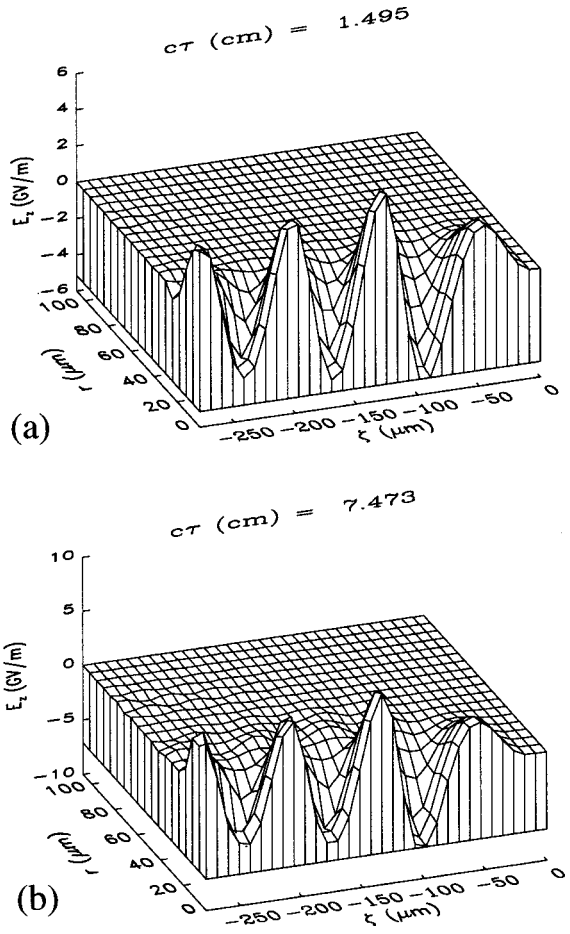

FIG. 10. Surface plot of the axial electric field $E_z(r,\zeta)$ for the simulation shown in Fig. 9.

gain over this distance is predicted to be $W_{ds}=(2/\pi)E_{ms}L_{ds}=0.45$ GeV.

When the simulation above is repeated with the pulse length reduced to 100 fs ($\alpha_r=0.4$), the wavelength reduced to 0.8 μm, and the power increased to 25 TW, there is a significant improvement in the performance quantities. The peak axial electric field E_{ms} averaged over an envelope oscillation is now 10.2 GV/m, the simulation dephasing length $L_{ds}=20.9$ cm, and the dephasing-limited energy $W_{ds}=1.36$ GeV. The analytical model values for these performance quantities are $E_m=10.2$ GV/m, $L_d=21.4$ cm, and $W_d=1.40$ GeV, so the agreement is excellent.

B. Channel-guided self-modulated laser wakefield accelerator

For a laser with a fixed pulse length τ_L the resonance condition in the standard LFWA requires that the on-axis density n_0 satisfy Eq. (7) with the resonance ratio $\alpha_r\sim0.5$. Most high power short pulse lasers have pulse lengths exceeding 200 fs. The corresponding resonant densities are less than $10^{17}\,\mathrm{cm}^{-3}$. Current methods for plasma channel generation do not extrapolate well to this lower density regime. In addition, the accelerating gradients in this lower density regime are much lower than those already achieved in higher density plasmas [1–6]. The successful high density LWFA experiments have been in the self-modulated regime [1–6]. In this regime, the laser power P_0 exceeds the critical power $P_r(\mathrm{GW})=17.4\lambda_p^2/\lambda^2$ for relativistic self-focusing, and the pulse is self-guided over many Rayleigh lengths. However, self-guided SM-LWFA experiments and simulations exhibit highly nonlinear behavior and generally produce poor quality beams with large energy spreads and large shot-to-shot variations [2,4–6,12,38].

In this section the possibility of a channel-guided SM-LFWA is investigated. If a laser pulse with $P_0<P_r$ is injected into a channel whose density is much larger than the resonant value, several plasma wavelengths will fit within the pulse, and the pulse is likely to self-modulate. The density channel provides the guiding in this case. Krall and Zigler [46] carried out LEM simulations of a channel-guided SM-LWFA but at much lower laser powers than those considered in this section.

The 400 fs long resonant LWFA simulation shown in Fig. 8 was carried out with a low density $n_0=1.94\times10^{16}\,\mathrm{cm}^{-3}$. Figures 11 and 12 are taken from a simulation with similar laser parameters but much higher plasma density. Here $P_0=13$ TW, $n_0=8\times10^{17}\,\mathrm{cm}^{-3}$, $r_{\mathrm{ch}}=150\,\mu$m, $r_0=40\,\mu$m, $\Delta n/n_0=1$, $\tau_L=400$ fs, and $\lambda=1\,\mu$m. The critical power $P_r=24$ TW at this density, so $P_0/P_r\approx0.5$. The resonant ratio $\alpha_r=3.6$, so the beam is likely to self-modulate at the plasma wavelength λ_p.

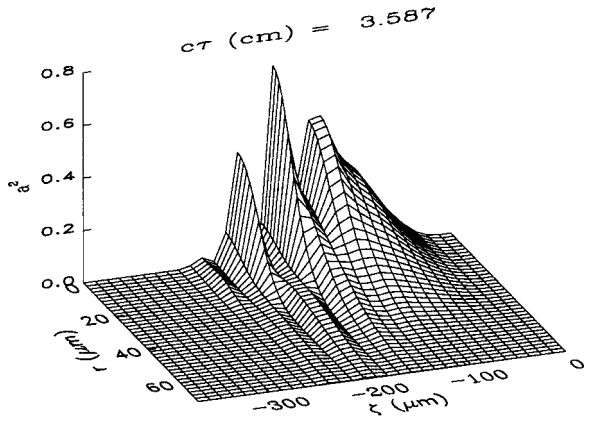

FIG. 11. Normalized intensity $a^2(r,\zeta)$ at $z=3.6\,\mathrm{cm}$ from a simulation of a channel-guided, self-modulated LWFA. Here $P_0=13\,\mathrm{TW}$, $n_0=8\times10^{17}\,\mathrm{cm}^{-3}$, $r_{\mathrm{ch}}=150\,\mu\mathrm{m}$, $r_0=40\,\mu\mathrm{m}$, $\Delta n/n_0=1$, $\tau_L=400\,\mathrm{fs}$, and $\lambda=1\,\mu\mathrm{m}$. The simulation exhibits self-modulation in the second half of the pulse.

Figure 11 plots the normalized intensity $a^2(r,\zeta)$ at $z=3.6\,\mathrm{cm}$. The pulse exhibits self-modulation in the second half of the pulse. A surface plot of the accelerating field E_z at the same location is shown in Fig. 12. The peak accelerating field is ~35 GV/m and occurs at $\zeta=-230\,\mu\mathrm{m}$. The same laser pulse propagating in a channel at the resonant density $\alpha_r=0.5$ or $n_0=2\times10^{16}\,\mathrm{cm}^{-3}$ would have produced an accelerating gradient of less than 1 GV/m. A similar simulation of the same laser pulse injected into a uniform plasma ($n_0=8\times10^{17}\,\mathrm{cm}^{-3}$, $\Delta n/n_0=0$) produced the expected expansion of the pulse spot size due to diffraction, and wakefield amplitudes decreased rapidly as the pulse propagated.

Similar effects may be produced at lower laser powers if the plasma density is raised. Figures 13 and 14 are taken from a simulation with $P_0=1.4\,\mathrm{TW}$, $n_0=5\times10^{18}\,\mathrm{cm}^{-3}$, $r_{\mathrm{ch}}=150\,\mu\mathrm{m}$, $r_0=20\,\mu\mathrm{m}$, $\Delta n/n_0=0.6$, $\tau_L=400\,\mathrm{fs}$, and $\lambda=1\,\mu\mathrm{m}$. For this simulation, $P_r=3.5\,\mathrm{TW}$ and $\alpha_r=9$. The injected radius r_0 is substantially lower than the matched radius $r_M=30\,\mu\mathrm{m}$, so the envelope oscillations in the laser spot size will be substantial.

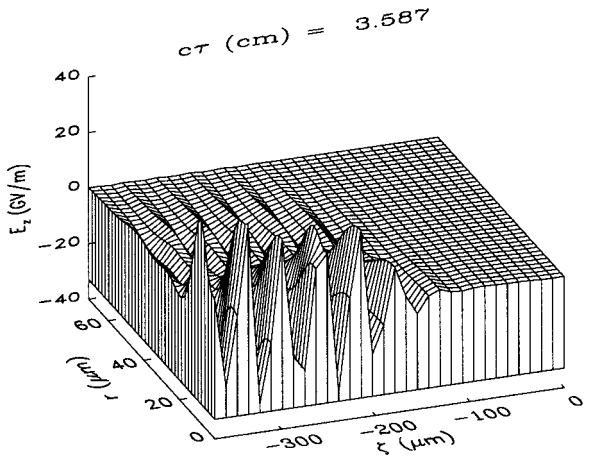

FIG. 12. Accelerating field $E_z(r,\zeta)$ at the same location from the simulation shown in Fig. 11. The peak accelerating field is ~35 GV/m and occurs at $\zeta=-230\,\mu\mathrm{m}$.

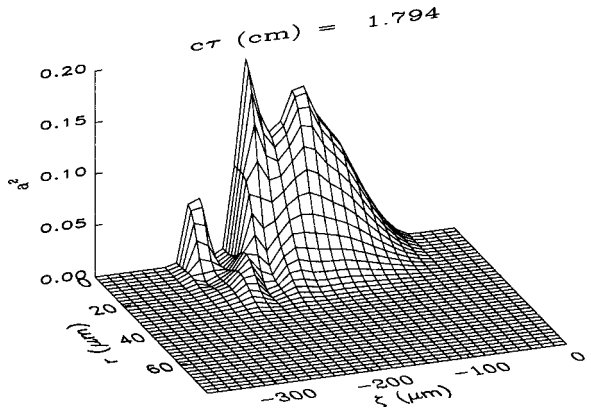

FIG. 13. Normalized intensity $a^2(r,\zeta)$ at $z=1.8\,\mathrm{cm}$ from a channel-guided SM-LWFA simulation with lower power and higher plasma density. Simulation parameters are $P_0=1.4\,\mathrm{TW}$, $n_0=5\times10^{18}\,\mathrm{cm}^{-3}$, $r_{\mathrm{ch}}=150\,\mu\mathrm{m}$, $r_0=20\,\mu\mathrm{m}$, $\Delta n/n_0=0.6$, $\tau_L=400\,\mathrm{fs}$, and $\lambda=1\,\mu\mathrm{m}$. The back of the pulse again exhibits self-modulation.

Figure 13 plots $a^2(r,\zeta)$ at $z=1.8\,\mathrm{cm}$; this position is near the exit of the 2 cm long capillary. The back of the pulse again exhibits self-modulation. The corresponding axial electric field $E_z(r,\zeta)$ is shown in Fig. 14. The peak accelerating gradient approaches 60 GV/m, and again the wakefield oscillations are regular and well defined. Although these fields are sufficient to produce substantial energy gain, it is likely that external injection of electrons would be required. The simulation parameters are similar to those produced in some of the high laser power shots reported by Kaganovich *et al.* [27]. The simulation results suggest that self-modulation of a guided laser pulse and large amplitude wakefields were probably produced in those experiments.

The channel-guided SM-LWFA has a number of attractive features. The channels are substantially easier to produce than those required for a resonant LWFA. Both the capillary discharge and axicon focus methods have been demonstrated experimentally at relatively high densities

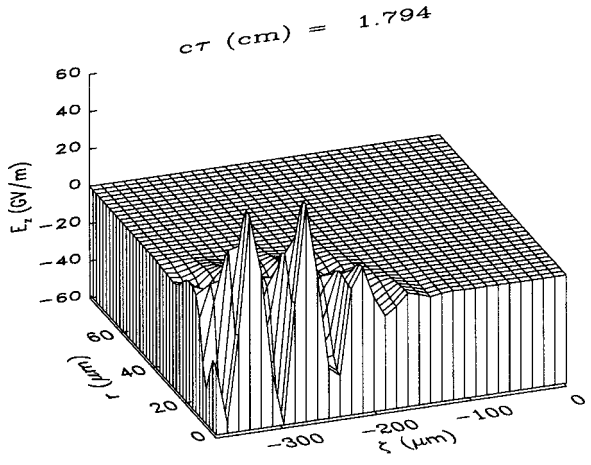

FIG. 14. Axial electric field $E_z(r,\zeta)$ from the simulation shown in Fig. 13. The peak accelerating gradient approaches 60 GV/m, and the wakefield oscillations are regular and well defined.

(10^{18}–$10^{19}\,\mathrm{cm}^{-3}$). The larger on-axis density also reduces the need for large $\Delta n/n_0$. (The simulations in Figs. 11–14 had $\Delta n/n_0 \sim 1$.) Because the plasma density is higher than in the resonant LWFA, accelerating gradients can also be substantially higher. It is expected that the channel guiding will result in cleaner wakefields and better beam quality than in the self-guided SM-LWFA experiments. However, since the self-modulation is still an inherently unstable process, this technique will probably produce poorer beam quality than a resonant LWFA. In addition, dephasing limitations are likely to play an important role because of the relatively high plasma density.

V. SUMMARY

The laser wakefield accelerator has emerged as a leading candidate for plasma-based, high gradient accelerators. The single stage energy gain can be enhanced substantially if some form of optical guiding of the laser pulse is provided. If the index of refraction $\eta(r)$ of the propagation medium is peaked on axis, the pulse may propagate at a small spot size over many Rayleigh lengths. A preformed plasma channel, in which the plasma density has an on-axis minimum, may provide the desired guiding effect, and channels generated by a capillary discharge, such as those described in Sec. II, have been used to guide tightly focused laser pulses over distances of several centimeters. Channel-guiding simulations using the 2D axisymmetric code LEM are consistent with both the theory and experiments.

The conventional or resonant LWFA regime, where $c\tau_L < \lambda_p$, offers the possibility of stable laser propagation and substantial electron acceleration but requires that some external form of optical guiding be provided. An analytical model is presented in Sec. III that predicts the performance of a channel-guided resonant LWFA in terms of primary laser and channel experimental parameters. The performance is quantified in terms of the peak accelerating gradient E_m, the dephasing length L_d, and the dephasing-limited energy gain W_d. The matched laser spot size r_M, plasma wavelength λ_p, and laser strength parameter a_0 are also expressed in terms of these primary parameters. The scaling laws provide a useful guide for future experiments and clearly illustrate some of the tradeoffs involved in choosing laser and channel parameters. For example, at very short pulse lengths, the plasma density is high, making it easier to generate the channel and confine the laser pulse to a small matched spot size. Although E_m can be very large, W_d is severely limited by dephasing. Longer pulse length lasers tend to have much lower accelerating gradients, in part because r_M is larger, thus reducing the laser intensity. However, the dephasing-limited energy gain is much larger.

Simulations of channel-guided resonant LWFAs generally agree well with the scaling model predictions. If the channel parameters are independent of z and the injection radius of the beam is close to r_M, the beam will propagate at a nearly constant spot size over long distances. Slippage of the plasma wake, which leads to dephasing, can be measured directly in the simulations, and agrees with the analytical predictions. As an example, a simulation with $\tau_L = 100\,\mathrm{fs}$, $\lambda = 0.8\,\mu\mathrm{m}$, $P_0 = 25\,\mathrm{TW}$, and appropriate channel parameters gave a predicted dephasing-limited energy gain $W_d = 1.36\,\mathrm{GeV}$, and excellent agreement with the scaling model.

Because of the experimental difficulties in producing laser and channel conditions necessary for a GeV-class resonant LWFA, the possibility of a *channel-guided* self-modulated LWFA was investigated. *Self-guided* SM-LWFA experiments have produced very high accelerating gradients but are highly unstable. If the same laser pulse is injected into a plasma channel at a somewhat lower plasma density, so that $P_0 < P_r$, the pulse may still self-modulate provided $c\tau_L/\lambda_p \gg 1$. The density channel provides the guiding in this case. Simulations in this regime produce a pulse that is well guided and eventually self-modulates. Accelerating gradients exceeding 10 GV/m may be produced.

The channel-guided SM-LWFA appears to be an interesting approach for near term experiments since the laser and channel requirements are less stressing than for a conventional LWFA, and the regime is likely to be less unstable than the self-guided SM-LWFA. In fact, simulations of the recent capillary discharge guiding experiment reported by Kaganovich *et al.* [27] suggest that self-modulation and large axial electric fields may have been produced in that experiment. However, the conventional LWFA remains the most appealing choice for a practical accelerator. Simulations indicate that long range propagation with little pulse distortion and nearly constant laser spot size and wakefield structure is possible over a wide range of parameters. The dephasing-limited energy gain can exceed 1 GeV over reasonable acceleration distances.

ACKNOWLEDGMENTS

Conversations with Y. Ehrlich, T. Jones, T. Antonsen, T. Hosokai, J. R. Peñano, D. F. Gordon, and E. Esarey are gratefully acknowledged. This work was supported by the Department of Energy, the Office of Naval Research, and the U.S.-Israeli Binational Science Foundation.

APPENDIX

Simulations of laser guiding in plasma channels have been carried out using the LEM code described by Sprangle *et al.* [13] and by Krall *et al.* [12]. LEM is a two-dimensional axisymmetric simulation that calculates laser fields and plasma response in a frame moving with the pulse at the speed of light. The independent variables in the simulation are r, $\zeta = z - ct$, and $\tau = t$. The laser-plasma interaction is described by the normalized potentials ϕ and $\mathbf{a}$, where $\phi = e\Phi/mc^2$, $\mathbf{a} = e\mathbf{A}/mc^2$, and Φ and $\mathbf{A}$ are the scalar and vector potentials. The model takes advantage of the separation in temporal and spatial scales for the fast laser oscillations (ω^{-1}, λ), the plasma response $(\omega_p^{-1}, \lambda_p)$, and the laser envelope $(Z_R/c, Z_R)$. Laser pulse evolution is described by a wave equation for $\hat{\mathbf{a}}_f$, the slowly varying amplitude of the normalized vector potential of the pulse. The fast time scale potential $\mathbf{a}_f = \hat{\mathbf{a}}_f \exp(ik_0\zeta)/2 + \mathrm{c.c.}$, where c.c. denotes the complex conjugate, and $k_0 = 2\pi/\lambda$.

The plasma is assumed to be a cold electron fluid with immobile ions, and relativistic corrections to the electron motion in the laser quiver field are explicitly retained. The quasistatic approximation is assumed, so the equations describing the plasma response neglect derivatives in τ and involve only r and ζ. In addition, both the laser spot size r_L and plasma wavelength λ_p are assumed to be much larger than the laser wavelength λ. As described in the Appendix of Ref. [12], it is possible to reduce the plasma response to a single equation of the form $\partial^2\psi/\partial\zeta^2 = G(\psi, |\hat{\mathbf{a}}_f|^2)$, where the normalized wake potential $\psi = \phi - a_z$, and G is a complicated function of the normalized potentials. The WAKE code developed by Mora and Antonsen [41,42] uses a similar approach to LEM and also employs the quasistatic approximation. WAKE also has an option to treat the plasma response with a kinetic model instead of a cold fluid model.

The simulation outputs laser and plasma quantities at fixed intervals of τ. It is convenient to use the laboratory coordinate z in place of $c\tau$ in describing output from the simulation since the characteristic time ($\sim Z_R/c$) for changes in the laser pulse is usually much less than the pulse duration τ_L. Since $\hat{\mathbf{a}}_f(r,\zeta,\tau)$ is calculated self-consistently, the pulse shape need not remain Gaussian, and the spot size r_L is not unambiguously defined. LEM defines r_L as the radius containing 84% of the beam power for a given beam slice; this reduces to the Gaussian radius defined in Eq. (2) if the profile remains Gaussian. The simulation also calculates a single characteristic spot size $r_L(z)$. This quantity is calculated at a reference point $\zeta^*(z)$ which moves at the nominal group velocity $\beta_{g0}c = (1 - \lambda^2/2\lambda_p^2)c$ of the pulse. In the simulation coordinate system, $d\zeta^*/dz = 1 - \beta_{g0}$. Group velocity slippage of the pulse imposes a major limitation on laser wakefield acceleration [4,7,34,39,44,45]. The actual slippage rate in simulation is usually somewhat faster than the nominal rate due to a finite spot size correction [34,45,50–53].

[1] K. Nakajima, D. Fisher, T. Kawakubo, H. Hashaniki, A. Ogata, Y. Kato, Y. Kitagawa, R. Kodama, K. Mima, H. Shiraga, K. Suzuki, K. Yamakawa, T. Zhang, Y. Sakawa, T. Shoji, Y. Nishida, N. Yagami, M. Downer, and T. Tajima, Phys. Rev. Lett. **74**, 4659 (1995).

[2] A. Modena, Z. Najmudin, A. E. Dangor, C. E. Clayton, K. A. Marsh, C. Joshi, V. Malka, C. B. Darrow, and C. Danson, IEEE Trans. Plasma Sci. **PS-24**, 289 (1996).

[3] D. Umsteader, S. Y. Chen, A. Maksimchuk, G. Mourou, and R. Wagner, Science **273**, 472 (1996).

[4] D. Gordon, K. C. Tzeng, C. E. Clayton, A. E. Dangor, V. Malka, K. A. Marsh, A. Modena, W. B. Mori, P. Muggli, Z. Najmudin, D. Neely, C. Danson, and C. Joshi, Phys. Rev. Lett. **80**, 2133 (1998).

[5] A. Ting, C. I. Moore, K. Krushelnick, C. Manka, E. Esarey, P. Sprangle, R. Hubbard, H. R. Burris, and M. Baine, Phys. Plasmas **4**, 1889 (1997).

[6] C. I. Moore, A. Ting, K. Krushelnick, E. Esarey, R. F. Hubbard, B. Hafizi, H. R. Burris, C. Manka, and P. Sprangle, Phys. Rev. Lett. **79**, 3909 (1997).

[7] T. Tajima and J. M. Dawson, Phys. Rev. Lett. **43**, 267 (1979).

[8] L. M. Gorbunov and V. I. Kirsanov, Zh. Eksp. Teor. Fiz. **93**, 509 (1987) [Sov. Phys. JETP **66**, 290 (1987)].

[9] P. Sprangle, E. Esarey, A. Ting, and G. Joyce, Appl. Phys. Lett. **53**, 2146 (1988).

[10] P. Sprangle and E. Esarey, Phys. Fluids B **4**, 2241 (1992).

[11] N. E. Andreev, L. M. Gorbunov, V. I. Kirsanov, A. A. Pogosova, and R. R. Ramazashvili, Pis'ma Zh. Eksp. Teor. Fiz. **55**, 551 (1992) [JETP Lett. **55**, 571 (1992)].

[12] J. Krall, A. Ting, E. Esarey, and P. Sprangle, Phys. Rev. E **48**, 2157 (1993); J. Krall, E. Esarey, P. Sprangle, and G. Joyce, Phys. Plasmas **1**, 1738 (1994).

[13] P. Sprangle, E. Esarey, J. Krall, and G. Joyce, Phys. Rev. Lett. **69**, 2200 (1992).

[14] A. B. Borisov, X. M. Shi, V. B. Karpov, O. B. Shiryaev, J. C. Solem, A. McPherson, K. Boyer, and C. K. Rhodes, J. Opt. Soc. Am. B **11**, 1941 (1994); A. B. Borisov, S. Cameron, Y. Dai, J. Davis, T. Nelson, W. A. Schroeder, J. W. Longworth, K. Boyer, and C. K. Rhodes, J. Phys. B **32**, 3511 (1999).

[15] F. Amiranoff, S. Baton, D. Bernard, B. Cros, D. Descamps, F. Dorchies, F. Jacquet, V. Malka, J. R. Marquès, G. Matthieussent, P. Miné, A. Modena, P. Mora, J. Morillo, and Z. Najmudin, Phys. Rev. Lett. **81**, 995 (1998); F. Dorchies, F. Amiranoff, V. Malka, J. R. Marques, A. Modena, D. Bernard, F. Jacquet, Ph. Mine, B. Cros, G. Matthieussent, P. Mora, A. Solodov, J. Morillo, and Z. Najmudin, Phys. Plasmas **6**, 2903 (1999).

[16] C. G. Durfee III and H. M. Milchberg, Phys. Rev. Lett. **71**, 2409 (1993); H. M. Milchberg, T. R. Clark, C. G. Durfee III, T. M. Antonsen, and P. Mora, Phys. Plasmas **3**, 2149 (1996).

[17] T. R. Clark and H. M. Milchberg, Phys. Rev. Lett. **78**, 2373 (1997).

[18] S. P. Nikitin, T. M. Antonsen, T. R. Clark, Y. L. Li, and H. M. Milchberg, Opt. Lett. **22**, 322 (1998).

[19] W. P. Leemans, P. Volfbeyn, K. Z. Gao, S. Chattopadhyay, C. B. Schroeder, B. A. Shadwick, P. B. Lee, J. S. Wurtele, and E. Esarey, Phys. Plasmas **5**, 1615 (1998).

[20] P. Volfbeyn and W. P. Leemans, in *Advanced Accelerator Concepts*, edited by W. Lawson, C. Bellamy, and D. F. Brosius, AIP Conf. Proc. No. **472** (AIP, Woodbury, NY, 1999), p. 514.

[21] P. Volfbeyn, E. Esarey, and W. P. Leemans, Phys. Plasmas **6**, 2269 (1999).

[22] E. W. Gaul, S. P. Le Blanc, and M. C. Downer, in Advanced Accelerator Concepts (Ref. [20]), p. 377; E. W. Gaul, S. P. Le Blanc, A. R. Rundquist, R. Zgadzaj, H. Lamghoff, and M. C. Downer, Appl. Phys. Lett. **77**, 4112 (2000).

[23] A. Zigler, Y. Ehrlich, C. Cohen, J. Krall, and P. Sprangle, J. Opt. Soc. Am. B **13**, 68 (1996).

[24] Y. Ehrlich, C. Cohen, A. Zigler, J. Krall, P. Sprangle, and E. Esarey, Phys. Rev. Lett. **77**, 4186 (1996).

[25] Y. Ehrlich, C. Cohen, D. Kaganovich, A. Zigler, R. F. Hubbard, P. Sprangle, and E. Esarey, J. Opt. Soc. Am. B **15**, 2416 (1998).

[26] D. Kaganovich, P. V. Sasarov, Y. Ehrlich, C. Cohen, and A. Zigler, Appl. Phys. Lett. **71**, 2295 (1997).
[27] D. Kaganovich, A. Ting, C. I. Moore, A. Zigler, H. R. Burris, Y. Ehrlich, R. Hubbard, and P. Sprangle, Phys. Rev. E **59**, R4769 (1999).
[28] R. F. Hubbard, Y. Ehrlich, D. Kaganovich, C. Cohen, C. I. Moore, P. Sprangle, A. Ting, and A. Zigler, in Advanced Accelerator Concepts (Ref. [20]), p. 394.
[29] D. Kaganovich, P. Sasorov, C. Cohen, and A. Zigler, Appl. Phys. Lett. **775**, 772 (1999).
[30] T. Hosokai, M. Kando, H. Dewa, H. Kotaki, S. Kondo, N. Hasegawa, K. Nakajima, and K. Horioka, Opt. Lett. **25**, 10 (2000).
[31] K. Krushelnick, A. Ting, C. I. Moore, H. R. Burris, E. Esarey, P. Sprangle, and M. Baine, Phys. Rev. Lett. **78**, 4047 (1997).
[32] P. Sprangle, E. Esarey, and J. Krall, Phys. Rev. E **54**, 4211 (1996).
[33] A. J. McKinnon, M. Borghesi, A. Iwase, M. W. Jones, G. J. Pert, S. Rae, K. Burnett, and O. Willi, Phys. Rev. Lett. **76**, 1473 (1996).
[34] P. Sprangle and B. Hafizi, Phys. Plasmas **6**, 1683 (1999).
[35] T. M. Antonsen and Z. Bian, Phys. Rev. Lett. **82**, 3617 (1999).
[36] W. B. Mori, C. D. Decker, D. E. Hinkle, and T. Katsouleas, Phys. Rev. Lett. **72**, 1482 (1994).
[37] W. B. Mori, IEEE J. Quantum Electron. **33**, 1942 (1997).
[38] K.-C. Tzeng, W. B. Mori, and T. Katsouleas, Phys. Rev. Lett. **79**, 5258 (1997).
[39] E. Esarey, B. Hafizi, R. Hubbard, and A. Ting, Phys. Rev. Lett. **80**, 5552 (1998).
[40] B. Hafizi, A. Ting, P. Sprangle, and R. F. Hubbard, Phys. Rev. E **62**, 4120 (2000).
[41] T. M. Antonsen and P. Mora, Phys. Rev. Lett. **69**, 2204 (1992); Phys. Fluids B **5**, 1440 (1993).
[42] P. Mora and T. M. Antonsen, Phys. Plasmas **4**, 217 (1997).
[43] P. Sprangle, E. Esarey, and A. Ting, Phys. Rev. A **41**, 4463 (1990).
[44] E. Esarey, P. Sprangle, J. Krall, and A. Ting, IEEE Trans. Plasma Sci. **24**, 252 (1996).
[45] R. F. Hubbard, P. Sprangle, and B. Hafizi, IEEE Trans. Plasma Sci. **28**, 1159 (2000).
[46] J. Krall and A. Zigler, Naval Research Laboratory Report No. 6790-95-7651, 1995 (unpublished).
[47] P. Sprangle, A. Ting, and C. M. Tang, Phys. Rev. Lett. **59**, 202 (1987); Phys. Rev. A **36**, 2773 (1987).
[48] E. Esarey, P. Sprangle, J. Krall, and A. Ting, IEEE J. Quantum Electron. **33**, 1879 (1997).
[49] E. Esarey, P. Sprangle, J. Krall, A. Ting, and G. Joyce, Phys. Fluids B **5**, 2690 (1993).
[50] E. Esarey, P. Sprangle, M. Pilloff, and J. Krall, J. Opt. Soc. Am. B **12**, 1695 (1995).
[51] P. Sprangle, B. Hafizi, and P. Serafim, Phys. Rev. Lett. **82**, 1173 (1999).
[52] E. Esarey and W. P. Leemans, Phys. Rev. E **59**, 1082 (1999).
[53] P. Sprangle, B. Hafizi, and P. Serafim, Phys. Rev. E **59**, 3614 (1999).
[54] E. Esarey, C. B. Schroeder, B. A. Shadwick, J. S. Wurtele, and W. P. Leemans, Phys. Rev. Lett. **84**, 3081 (2000).
[55] P. Sprangle, B. Hafizi, and J. R. Peñano, Phys. Rev. E **61**, 4381 (2000).
[56] S. Jackel, R. Burris, J. Grun, A. Ting, C. Manka, K. Evans, and K. Kosakowskii, Opt. Lett. **20**, 1086 (1995).
[57] D. Korobkin, A. Goltsov, A. Morozov, and S. Suckewer, Phys. Rev. Lett. **81**, 1607 (1998).